Polymer Testing 110 (2022) 107568

Contents lists available at ScienceDirect

Polymer Testing

journal homepage: www.elsevier.com/locate/polytest

Effect of crystal structure on nanofiber morphology and chemical modification; design of CeO_2/PVDF membrane

Adam Verner [a,b,*], Jonáš Tokarský [a,c], Pavla Čapková [d], Petr Ryšánek [d], Oldřich Benada [d,e], Jiří Henych [f,g], Jakub Tolasz [f,g], Martin Kormunda [d], Michal Syrový [d]

[a] Nanotechnology Centre, CEET, VŠB-Technical University of Ostrava, 17. listopadu 2172/15, 708 00, Ostrava-Poruba, Czech Republic
[b] ENET Centre, CEET, VŠB–Technical University of Ostrava, 17. listopadu 2172/15, 708 00, Ostrava-Poruba, Czech Republic
[c] Institute of Environmental Technology, CEET, VŠB–Technical University of Ostrava, 17. listopadu 2172/15, 708 00, Ostrava-Poruba, Czech Republic
[d] Faculty of Science, Jan Evangelista Purkyně University, Pasteurova 3632/15, 400 96, Ústí nad Labem, Czech Republic
[e] Institute of Microbiology of the Czech Academy of Sciences, Vídeňská 1083, 142 20, Prague 4, Czech Republic
[f] Institute of Inorganic Chemistry of the Czech Academy of Sciences, 250 68, Husinec-Řež, Czech Republic
[g] Faculty of Environment, Jan Evangelista Purkyně University, Pasteurova 3632/15, 400 96, Ústí nad Labem, Czech Republic

ARTICLE INFO

Keywords:
Polyvinylidene fluoride
CeO_2
Nanofiber
Structure
Morphology
Molecular simulation

ABSTRACT

Layered crystal structures tend to form flat platelet-like crystallites, and nanofibers having such a structure exhibit strip-like morphology. Crystallographic plane forming the dominant flat surface of the nanofibers can be used for surface modification with catalytically active nanoparticles capable of anchoring to the dominant flat surface. In this study, polyvinylidene fluoride (PVDF) nanofibers exhibiting strip-like morphology and longitudinal folding were prepared using wire electrospinning, and surface modified with CeO_2 nanoparticles. Experimental characterization of the CeO_2/PVDF membrane using (high-resolution) scanning electron microscopy and X-ray photoelectron spectroscopy was supplemented by a force field-based molecular modeling. The modeling has shown that the dominant PVDF(100) plane is suitable for anchoring the CeO_2 nanoparticles. In this respect, the PVDF(100) plane is comparable to the less exposed fluorine-oriented PVDF(010) plane, and both planes show stronger interaction with CeO_2 compared to hydrogen-oriented PVDF(010) plane. Molecular modeling also revealed preferred crystallographic orientations of anchored CeO_2 nanoparticles: these are the catalytically active planes (100), (110), and (111). The successful surface modification and the finding that CeO_2 nanoparticles on the dominant PVDF(100) surface can preferentially exhibit these crystallographic orientations thus provides the possibility of various practical applications of the CeO_2/PVDF membrane.

1. Introduction

In recent decades, many articles have been published on electrospinning technology and the influence of technological parameters on the properties of nanofiber membranes [1–5], especially those made from polyvinylidene fluoride (PVDF) [6–14]. However, less attention has been paid to the effect of crystal structure on morphology and properties. Electrostatic spinning leads to a specific microstructure of polymeric nanofibrous materials. A characteristic feature of this microstructure is the preferred orientation of the polymer chains in the crystal structure of the nanofibers in the direction of the fiber axis. The effect of polymer chains ordering and nanofiber morphology has been reported by Gazzano et al. [15], who found an interesting relationship between ordering of chains, fiber diameter, degree of crystallinity, and degree of chain alignment. Gazzano et al. [15] presented fiber diameters for polyethylene oxide, polyacrylonitrile, and nylon 6,6 (all of which were prepared in the same way), and showed that polyacrylonitrile (PAN) fibers exhibit the highest diameter. This indicates the effect of a layered crystal structure that forms stripe-like fibers with a tendency to longitudinally twist into hollow tubes, as recently described by Ryšánek et al. [16] for PAN.

It is generally known that layered crystal structures form flat platelet-like crystallites. In our recent work [16] we have shown by the example of PAN that this rule also applies to the crystallization of polymeric electrospun nanofibers. Flat stripe-like PAN nanofibers rolled lengthwise forming hollow fibers, exhibiting a larger fiber diameter than

* Corresponding author. Nanotechnology Centre, CEET, VŠB-Technical University of Ostrava, 17. listopadu 2172/15, 708 00, Ostrava-Poruba, Czech Republic.
E-mail address: adam.verner@vsb.cz (A. Verner).

https://doi.org/10.1016/j.polymertesting.2022.107568
Received 8 January 2022; Received in revised form 28 March 2022; Accepted 31 March 2022
Available online 4 April 2022

e.g. nylon prepared under the same conditions. PAN and β-PVDF phase are both similar crystal structures, where polymer chains are arranged in layers with acentric charge distribution. That means PVDF electrospun nanofibers consisting of β-PVDF phase [8] are another candidate for the formation of flat stripe-like morphology. The stripe-like nanofiber morphology can also affect the chemical modification (especially the adhesion of metal oxide nanoparticles) when the flat nanofiber surface is preferably formed by a certain type of crystal plane. In this work, this effect using cerium oxide nanoparticles (CeO_2 NPs) was studied.

CeO_2 NPs have been chosen as a model structure for this purpose due to their unique properties described in many papers (see reviews [17, 18]). The application potential of CeO_2 NPs is very wide; from catalytic [19–25] and photocatalytic [26–31] properties, through degradation of toxic hardly degradable pollutants [32–37] to medical use [38–42]. Therefore, the manufacturing of CeO_2NPs/PDVF membrane is a good opportunity to utilize both the stripe-like morphology of β-PVDF fibers and the unique properties of CeO_2 NPs.

However, to achieve this goal, CeO_2 NPs must be able to anchor to the dominant flat surface of the nanofibers. In our study, the fulfillment of this condition was investigated by a combination of experiments (SEM + HRSEM microscopy and XPS spectroscopy) with molecular modeling (force field calculations) in Biovia Materials Studio 7.0 modeling environment.

2. Experimental

2.1. CeO_2NPs/PVDF membranes: materials and technology

The fabrication of CeO_2NPs/PVDF membranes was performed in two steps: electrospinning of PVDF membranes with subsequent modification by CeO_2 NPs. The spinning solution was prepared using PVDF SOLEF® 6020/1001 powder (purity >99.9%; CAS no. 24937-79-9) from Solvay Company [43] by dissolving and gentle stirring the PVDF for 24 h at the temperature of 25 °C in dimethylformamide solvent, so the 12% solution (w/w) was prepared. Electrospinning using wire spinning device NS 1WS500U (Nanospider laboratory device from Elmarco, Czech Republic) has been carried out under the following conditions: applied voltage 60 kV, electrode distance 180 mm, the temperature in spinning chamber 25 °C, and relative humidity 34%.

CeO_2 NPs for modification of the PVDF membranes were prepared using a low-temperature one-pot synthesis described recently by Tolasz et al. [44]. Modification of the PVDF membranes with CeO_2 NPs was performed simply by immersion of the PVDF membranes in a colloidal water solution of CeO_2 NPs (c = 0.1 g/L) for 1 min. The resulting CeO_2NPs/PVDF membranes were air-dried at room temperature overnight.

2.2. Characterisation of samples

SEM analysis was carried out using the FEI Nova NanoSEM 450 scanning electron microscope (FEI, Brno, Czech Republic) operating at 3 kV (CBS detector in B + C mode). When sample charging occurred, a beam deceleration mode of the device with specimen negative bias of 500 V was used to minimize sample charging and improve the image contrast [45]. The EDS standardless semiquantitative analysis was performed on the FEI Nova NanoSEM 450 scanning electron microscope operating at 15 kV with ETD/TLD detectors using an Ultim Max 100 SDD detector and AZtecLive software (Oxford Instruments; Abingdon-on-Thames, The United Kingdom).

X-ray photoelectron spectroscopy (XPS) as the most important tool in the analysis of surface chemistry was used to confirm the presence of CeO_2 NPs on the PVDF membrane, and to estimate the CeO_2 concentration on membranes. SPECS Phoibos 100 X-ray photoelectron spectrometer operating in FAT mode with SPECS XR50 Al/Mg X-ray tube was used for XPS spectra. The high-resolution spectra for the quantitative analysis were obtained with 10 eV pass energy and X-ray from Al anode. The Mg anode was used to identify Auger peaks.

2.3. Atomistic models of CeO_2NPs/PVDF membranes; modeling strategy

Building of initial models, geometry optimizations, and energy calculations were carried out in Biovia Materials Studio 7.0 (MS) modeling environment. Since electrospun PVDF nanofibers crystalize in the β-PVDF phase structure, data for this phase were used to build the atomistic model of the membrane. Crystal structure of the β-PVDF phase has been determined by Hasegawa et al. [46] as orthorhombic, space group Cm2m, with cell parameters: a = 8.58 Å, b = 4.91 Å, and c = 2.56 Å (Fig. 1a). Distinctly layered ordering of polymer chains in the crystal structure of β-PVDF phase is illustrated in Fig. 1b. Periodic models of PVDF(100), fluorine-oriented PVDF(010) (denoted as PVDF(010)F), and hydrogen-oriented PVDF(010) (denoted as PVDF(010)H) surfaces were created by cleaving the structure along corresponding (hkl) planes (see Fig. 1b). The resulting surfaces were enlarged to ~100 × 100 Å and finished by the addition of a vertical vacuum slab with a height of 400 Å (Fig. S1 in the *Supplementary material*).

CeO_2 cubic unit cell having lattice parameter a = 5.411 Å (Fig. 2) was built according to Wyckoff [47]. Bases of CeO_2 NPs were created by cleaving the CeO_2 structure along the following (hkl) planes: (100), (110), (111), and (211). Through these planes, the CeO_2 NPs were adjacent to the PVDF surfaces. In the case of alternate occupation of (hkl) planes only by Ce atoms or only by O atoms, both variants were prepared and distinguished by Ce or O (i.e. (111)Ce, (111)O, (100)Ce, and (100)O; Fig. 2). Each model of CeO_2 NP contained 594 atoms ($Ce_{198}O_{396}$).

Eighteen initial NP/surface models were prepared by placing each of the six CeO_2 NPs on each of the three PVDF surfaces. The NPs were oriented with the base parallel to a given PVDF surface. Five variants of each initial NP/surface model were built, so a total of ninety models were studied. Geometry optimization of each model was performed in MS/Forcite module. Examples of initial and optimized models are provided in the *Supplementary material* (Fig. S2). Atoms were parameterized and their charges were assigned by COMPASS force field [48], which was verified for use on models containing either CeO_2 NP or PVDF. Mei et al. [49] simulated interactions of CeO_2 and silane coupling agent in solution using COMPASS force field. The same force field was also used by Bahlakeh et al. [50] in work focused on CeO_2 NP on polyester resin. Zeng et al. [51] used COMPASS for simulations on the disintegration of PVDF, and Satyanarayana et al. [52] used this force field to simulate α- and β-PVDF phase changes.

The Smart algorithm, as implemented in the MS, with $5{\cdot}10^5$ steps was used. Convergence thresholds for energy, force, and displacement were $1{\cdot}10^{-4}$ kcal mol^{-1}, $5{\cdot}10^{-3}$ kcal mol^{-1} Å^{-1}, and $5{\cdot}10^{-5}$ Å, respectively. Cell parameters were not optimized. For each optimized model, interaction energy (E_{int}; kcal/mol) was calculated from potential energies (E_p) using the following equation

$$E_{int} = E_{p1} - E_{p2} - E_{p3}$$

where E_{p1} is E_p of a whole model, E_{p2} is E_p of a PVDF surface, and E_{p3} is E_p of a CeO_2 NP. Interaction energy values were related to 1 nm^2 and denoted as E_{int}/S (kcal mol^{-1} nm^{-2}). The lower the Eint/S value, the stronger the interaction between CeO_2 NP and PVDF surface.

3. Results and discussion

3.1. SEM and XPS analyses

SEM and HRSEM images (CBS detector in B + C mode) of PVDF nanofibers (Fig. 3a–d) revealed their markedly flattened cross-section. This is especially evident in the case of twisting fibers showing both their main flat surfaces and significantly narrower edges (indicated by vertical white arrows). Concerning the structure of the β-PVDF phase

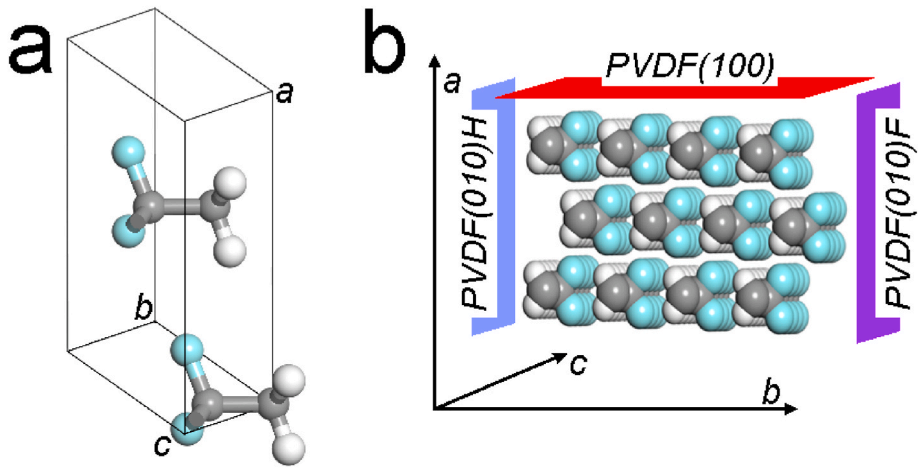

Fig. 1. (a) Unit cell of β-PVDF. (b) Layered ordering of chains in the β-PVDF crystal structure with marked positions of three main planes parallel to the c axis, i.e. parallel to the carbon backbone of the chains (b). Atom color legend: grey – C, light blue – F, white – H. (For interpretation of the references to color in this figure legend, the reader is referred to the Web version of this article.)

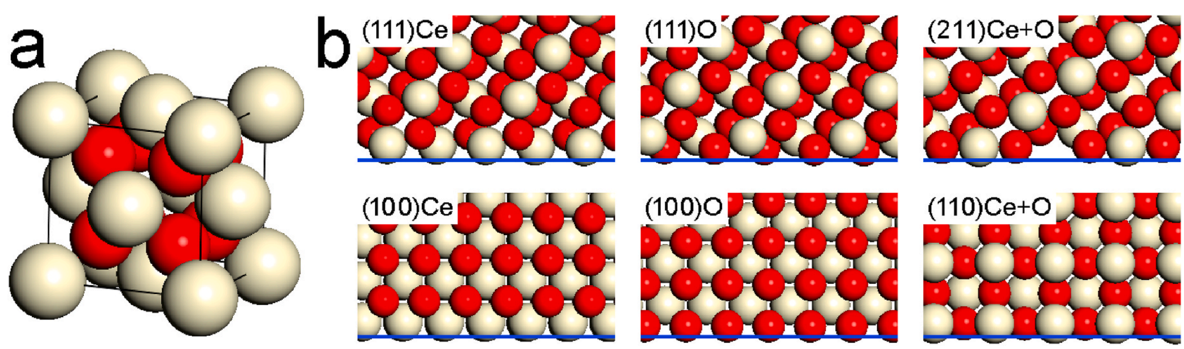

Fig. 2. (a) CeO_2 unit cell. (b) Side views of CeO_2 structure cleaved along (hkl) planes (111), (211), (100), and (110). The planes and atoms in them (forming the base of the NP adjacent to the PVDF surface) are marked with a blue line. Alternating Ce and O atoms are demonstrated for (111) and (100) planes. Both Ce + O atoms in one (110) or one (211) plane are clearly seen. (For interpretation of the references to color in this figure legend, the reader is referred to the Web version of this article.)

(Fig. 1), it can be concluded that the PVDF(100) plane exhibiting the layered structure corresponds to the surface of nanofibers. Another property of nanofibers observable in Fig. 3a–d is their longitudinal folding (indicated by horizontal white arrows) creating the effect of "hollow" fibers. This bending caused by the charge distribution in the structure of the PVDF chains (strongly electronegative F atoms only on one side of the carbon backbone; see Fig. 1) has been previously described also for the PAN structure [16].

The flatness of PVDF nanofibers is also documented on SEM images (TLD detector in SE mode) of PVDF (Fig. 4a) and CeO_2NPs/PVDF (Fig. 4b) samples. The convincing example of the CeO_2 covering the PVDF is available in Fig. 4b. The CeO_2 layer is not smooth, it is clearly structured, composed of agglomerated CeO_2 NPs. EDS analysis (Fig. 4c) performed on the CeO_2NPs/PVDF sample shows the presence of CeO_2, and the Ce:O weight percent ratio obtained (36.4 wt%: 8.7 wt% = 4.18) is in good agreement with the ideal Ce:O weight percent ratio in a stoichiometric CeO_2 (81.41 wt%: 18.59 wt% = 4.38).

XPS analysis (Fig. 5) confirmed the presence of CeO_2 NPs on PVDF fiber surfaces exhibiting an atomic concentration of Ce atoms on fiber surface layer 1.6 at.% just corresponding to the way of preparation, and oxygen atomic concentration 8.2 at.%. Oxygen concentration is relatively higher due to the surface impurities. The comparison of XPS spectral profiles Ce3d for pristine CeO_2 NPs and CeO_2NPs/PVDF membrane (Fig. 5) shows the same character confirming the presence of CeO_2 NPs on the PVDF surface. The additional peak in CeO_2NPs/PVDS spectra about binding energy 920 eV was confirmed to be the Auger peak.

3.2. Molecular modeling

Molecular modeling has shown the possibility of CeO_2 NPs anchoring on the surface of PVDF nanofibers. Negative E_{int}/S values were obtained for all examined CeO_2 planes on all examined PVDF planes (Table 1). Interactions between CeO_2 NPs and planes PVDF(100) and PVDF(010)F are comparable, and stronger compared to the interactions between CeO_2 NPs and PVDF(010)H plane (Table 1).

This is due to the fact, that PVDF(100) and PVDF(010)F contains contact atoms F providing strong hydrogen bonds with Ce atoms of the NP, because of the highest difference in electronegativity values (χ_F-χ_{Ce} = 2.86 [53]) within the possible interacting atomic pairs. For other interacting atomic pairs, the differences in electronegativity values are as follows: χ_H-χ_{Ce} = 1.08, χ_F-χ_O = 0.54 and χ_O-χ_H = 1.24 [53].

Contact atoms of the PVDF(010)H plane are hydrogens. Therefore, interaction with the oxygen atoms belonging to the NP structure is stronger than the interaction with the cerium atoms (χ_O-χ_H = 1.24 > χ_H-χ_{Ce} = 1.08).

Concerning the morphology of PVDF nanofibers (Figs. 3 and 4), it can be stated that the dominant surface is the layered PVDF(100) plane, while the available area of the other two PVDF planes is significantly smaller. In addition, in the case of longitudinal folding of the nanofibers, the resulting edges are also formed by the PVDF(100) plane. The anchoring of CeO_2 NPs to PVDF nanofibers is therefore controlled mainly by the interaction between CeO_2 NPs and PVDF(100) plane (see Fig. S2 in the *Supplementary material*). The remaining two planes do not

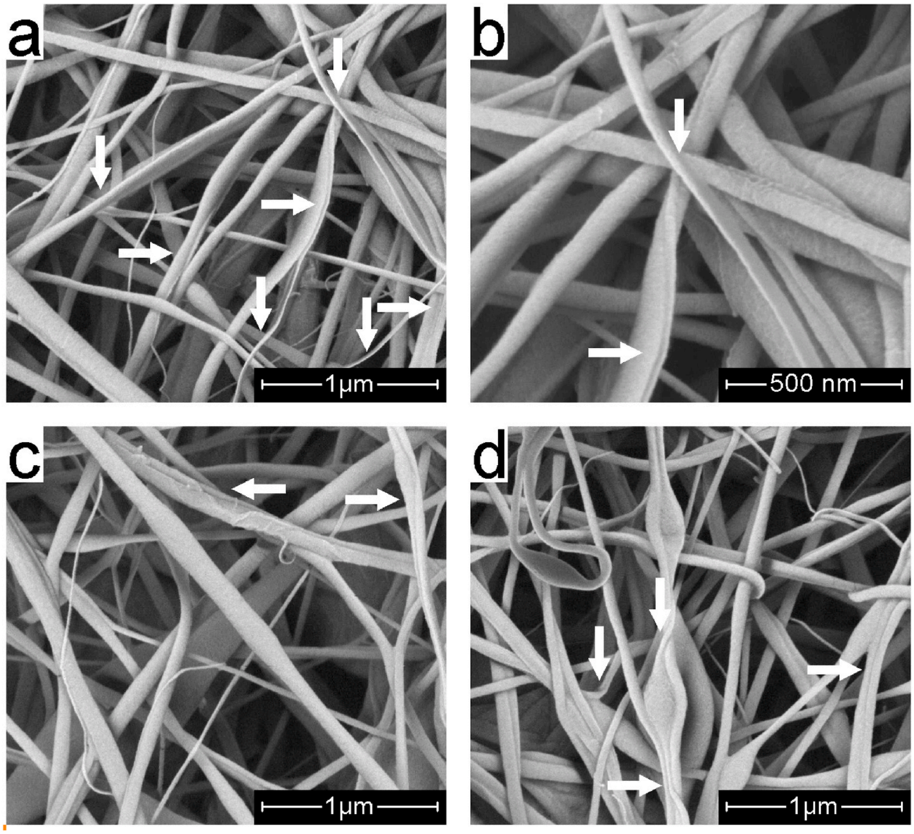

Fig. 3. SEM images (CBS detector in B + C mode) of the PVDF membrane showing a stripe-like morphology of the nanofibers. Narrower edge compared to the dominant flat surface and the longitudinal folding of nanofibers is indicated by vertical and horizontal white arrows, respectively. Image (b) provides a detailed view of the upper right quarter of image (a).

play much of a role in the real sample, neither the strongly interacting PVDF(010)F plane nor the weakly interacting PVDF(010)H plane.

CeO_2 NPs having a crystallographic orientation (211) exhibit the weakest interaction with each of the PVDF planes (Table 1). However, in the case of the dominant PVDF(100) plane, none of the remaining three CeO_2 planes (111), (110), and (100) is significantly preferred (Table 1), and CeO_2 NPs may therefore exhibit all of these crystallographic orientations in the CeO_2NPs/PVDF sample.

This result is promising because these CeO_2 planes are useful for their catalytic activity. Stubenrauch et al. [23] described the catalytic performance of (111) and (100) planes in the decomposition of formic acid and acetic acid. High reactivity of (110) and (100) planes for CO oxidation was reported by various authors, e.g. Tana et al. [22] and references therein. The catalytic activity of (100) plane for benzene oxidation was reported by Wang et al. [24]. Planes (110) and (100) are typical of the surface of CeO_2 nanorods, while in the case of CeO_2 nanoparticles, the surface is dominated by the (111) plane. This plane is the most energetically stable, and thus shows weaker catalytic properties than the other two, yet its catalytic efficiency has been demonstrated in hydrolysis [20] and the synthesis of dimethyl carbonate [25]. Photocatalytic properties have also been demonstrated in the reduction of CO_2 at the CeO_2 planes (110) and (100) [26] and in the production of hydrogen at the (111) plane [27].

Finding that CeO_2 NPs on the dominant β-PVDF(100) surface can preferentially exhibit these crystallographic orientations thus provides the possibility of various practical applications of the CeO_2NPs/PVDF membrane.

4. Conclusions

Wire electrospinning was utilized for the preparation of a non-woven membrane consisting of β-PVDF nanofibers. These nanofibers exhibit a strip-like morphology with the dominant flat surface formed by the β-PVDF(100) crystallographic plane. The membrane was surface modified with CeO_2 NPs. The presence of CeO_2 NPs on the surface of β-PVDF fibers was confirmed by SEM and XPS analyses. In addition to the experimental characterization, molecular modeling using a force field was also involved to compare the non-bond interactions of CeO_2 and PVDF structures for different mutual crystallographic orientations. The molecular modeling revealed that the β-PVDF(100) plane forming the dominant flat surface of the nanofibers is suitable for anchoring CeO_2 NPs. The interaction energies found for this plane are comparable to the interaction energies found for the β-PVDF(010)F plane. Weaker interactions with CeO_2 were found for the β-PVDF(010)H plane. Both β-PVDF(010)F and β-PVDF(010)H planes forming the edges of the flat nanofibers represent a significantly smaller surface area compared to the dominant β-PVDF(100) plane. Moreover, due to the longitudinal folding of the nanofibers, these planes come into contact, making them even less accessible for CeO_2 NPs. The interaction energy between CeO_2 and the β-PVDF(100) plane is thus the most important factor influencing the surface modification of the nanofibers by the CeO_2 NPs. The results of molecular modeling support the conclusion made on the basis of SEM analysis, i.e. the surface modification of PVDF nanofibers with CeO_2 NPs is possible, and the CeO_2NPs/PVDF sample is not just a mechanical mixture of both materials.

Molecular modeling revealed that CeO_2 NPs on the dominant β-PVDF (100) surface can preferentially exhibit the following three crystallographic orientations: (100), (110), (111). This is a promising result because these three CeO_2 planes are catalytically active.

The CeO_2NPs/PVDF membrane is a type of material useful in applications that require a nanostructured polymeric carrier surface-modified with catalytically active NPs with suitable crystallographic

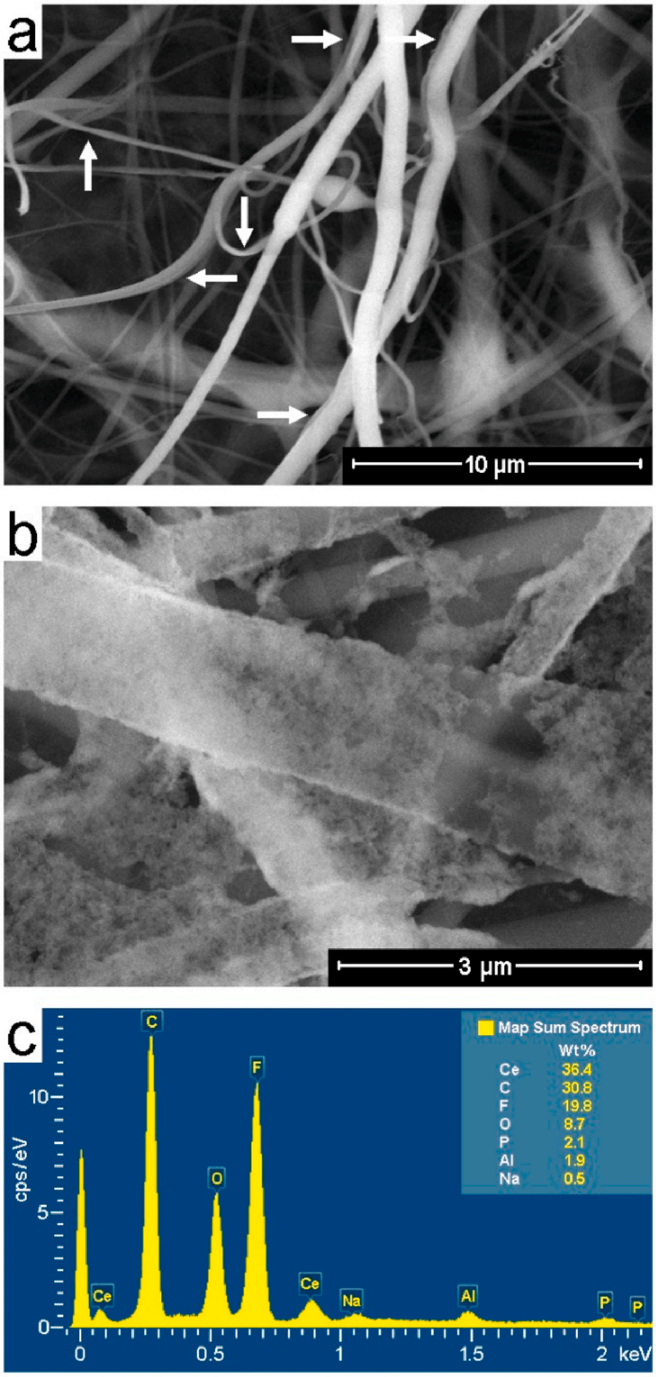

Fig. 4. SEM images (TLD detector in SE mode) of (a) the PVDF and (b) the CeO_2NPs/PVDF samples. (c) EDS analysis of the CeO_2NPs/PVDF sample.

orientations. The molecular modeling method described in this study is not limited to CeO_2 NPs and PVDF nanofibers - it can be used to study interactions and preferred crystallographic orientations of different NPs on different nanofibers.

Authors contribution

Adam Verner: Investigation, Data Curation, Writing - Original Draft, Visualization. Jonáš Tokarský; Methodology, Validation, Investigation, Data Curation, Writing - Original Draft, Writing - Review & Editing, Visualization, Supervision, Funding acquisition. Pavla Čapková; Conceptualization, Writing - Original Draft, Supervision, Funding acquisition. Petr Ryšánek: Investigation. Oldřich Benada: Investigation. Jiří Henych: Investigation, Writing - Review & Editing. Jakub Tolasz: Investigation. Martin Kormunda: Investigation, Writing - Review & Editing. Michal Syrový; Investigation.

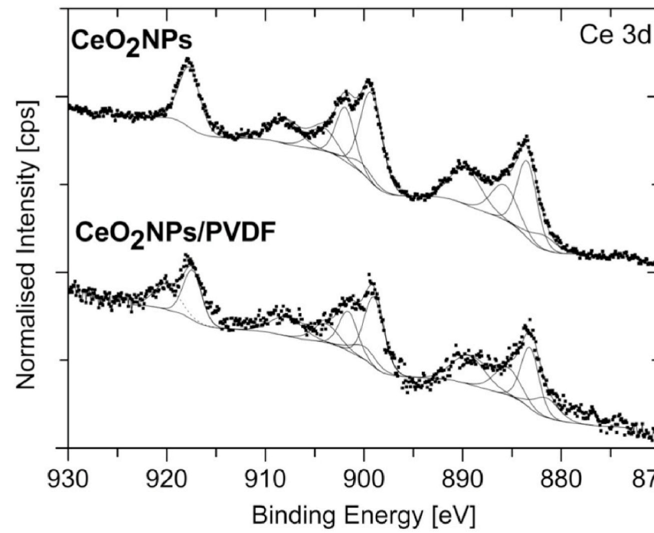

Fig. 5. XPS spectral profiles Ce3d for samples CeO_2 NPs and CeO_2NPs/PVDF.

Table 1
E_{int}/S (kcal/mol/nm^2) values for each of the four CeO_2 planes adjacent to each of the three PVDF planes. In the case of CeO_2 planes (111) and (100), E_{int}/S values are provided for both types of adjacent atoms, and also the average of both E_{int}/S values is provided in the last column. The E_{int}/S values for planes (110) and (211) are provided in column Ce + O.

CeO_2 adjacent planes	PVDF adjacent planes	adjacent atoms			
		Ce	O	Ce + O	average
(111)	(100)	−2619 ± 62	−2297 ± 65	–	−2458 ± 181
(100)	(100)	−2479 ± 62	−2441 ± 155	–	−2460 ± 120
(100)	(100)	–	–	−2412 ± 139	–
(211)	(100)	–	–	−1 687 ± 27	–
(111)	(010)F	−3073 ± 92	−2285 ± 93	–	−2679 ± 405
(100)	(010)F	−2868 ± 92	−1731 ± 143	–	−2300 ± 581
(110)	(010)F	–	–	−2234 ± 71	–
(211)	(010)F	–	–	−1732 ± 53	–
(111)	(010)H	−1792 ± 130	−1806 ± 68	–	−1799 ± 104
(100)	(010)H	−1584 ± 132	−2467 ± 49	–	−2025 ± 453
(110)	(010)H	–	–	−1928 ± 86	–
(211)	(010)H	–	–	−1485 ± 61	–

Declaration of competing interest

The authors declare that they have no known competing financial interests or personal relationships that could have appeared to influence the work reported in this paper.

Acknowledgements

Funding: This work was supported by The Ministry of Education, Youth and Sports of the Czech Republic via the SGS - Grant Agency of the VŠB-TUO and the Internal Grant Agency of the J. E. Purkyně University in Ústí nad Labem [grant numbers SP2020/24, UJEP-SGS-2019-53-006-3]; authors acknowledge the assistance provided by the Research Infrastructure NanoEnviCz and ProNanoEnviCz projects [grant numbers LM2018124, CZ.02.1.01/0.0/0.0/18_046/0015586]; the project ERDF/ESF UniQSurf - Centre of biointerfaces and hybrid functional materials [grant number CZ.02.1.01/0.0/0.0/17_ 048/0007411] and the Doctoral grant competition VSB - Technical University of Ostrava within the Operational Programme Research, Development and Education, under project DGS/TEAM/2020-007 [grant number CZ.02.2.69/0.0/0.0/19_073/0016945].

Appendix A. Supplementary data

Supplementary data to this article can be found online at https://doi.org/10.1016/j.polymertesting.2022.107568.

References

[1] R. Gopal, S. Kaur, Z. Ma, C. Chan, S. Ramakrishna, T. Matsuura, Electrospun nanofibrous filtration membrane, J. Membr. Sci. 281 (2006) 581–586, https://doi.org/10.1016/j.memsci.2006.04.026.
[2] B. Zaarour, L. Zhu, X. Jin, A Review on the secondary surface morphology of electrospun nanofibers: formation mechanisms, characterizations, and applications, ChemistrySelect 5 (2020) 1335–1348, https://doi.org/10.1002/slct.201903981.
[3] Z.-M. Huang, Y.-Z. Zhang, M. Kotaki, S. Ramakrishna, A review on polymer nanofibers by electrospinning and their applications in nanocomposites, Compos. Sci. Technol. 63 (2003) 2223–2253, https://doi.org/10.1016/S0266-3538(03)00178-7.
[4] P. Čapková, A. Čajka, Z. Kolská, M. Kormunda, J. Pavlík, M. Munzarová, M. Dopita, D. Rafaja, Phase composition and surface properties of nylon-6 nanofibers prepared by nanospider technology at various electrode distances, J. Polym. Res. 22 (2015) 101, https://doi.org/10.1007/s10965-015-0741-3.
[5] P. Ryšánek, M. Malý, P. Čapková, M. Kormunda, Z. Kolská, M. Gryndler, O. Novák, L. Hocelíková, L. Bystrianský, M. Munzarová, Antibacterial modification of nylon-6 nanofibers: structure, properties and antibacterial activity, J. Polym. Res. 24 (2017) 208, https://doi.org/10.1007/s10965-017-1365-6.
[6] E.S. Cozza, O. Monticelli, E. Marsano, P. Cebe, On the electrospinning of PVDF: influence of the experimental conditions on the nanofiber properties, Polym. Int. 62 (2013) 41–48, https://doi.org/10.1002/pi.4314.
[7] K. Gao, X. Hu, C. Dai, T. Yi, Crystal structures of electrospun PVDF membranes and its separator application for rechargeable lithium metal cells, Mater. Sci. Eng. B 131 (2006) 100–105, https://doi.org/10.1016/j.mseb.2006.03.035.
[8] P. Čapková, M. Kormunda, Z. Kolská, J. Trögl, M. Munzarová, P. Ryšánek, Electrospun antimicrobial PVDF-DTAB nanofibrous membrane for air filtration: effect of DTAB on structure, morphology, adhesion, and antibacterial properties, Macromol. Mater. Eng. 303 (2018) 1700415, https://doi.org/10.1002/mame.201700415.
[9] G. Kang, Y. Cao, Application and modification of poly(vinylidene fluoride) (PVDF) membranes – a review, J. Membr. Sci. 463 (2014) 145–165, https://doi.org/10.1016/j.memsci.2014.03.055.
[10] A. Bottino, G. Capannelli, A. Comite, Novel porous poly(vinylidene fluoride) membranes for membrane distillation, Desalination 183 (1–3) (2005) 375–382, https://doi.org/10.1016/j.desal.2005.03.040.
[11] W. Bing, K. Li, W.K. Teo, Preparation and characterization of polyvinylidene fluoride hollow fiber membranes for vacuum membrane distillation, J. Appl. Polym. Sci. 106 (3) (2007) 1482–1495, https://doi.org/10.1002/app.26624.
[12] F. Liu, H. Awanis Hasim, Y. Liu, M.R. Moghareh Abed, K. Li, Progress in the production and modification of PVDF membranes, J. Membr. Sci. 375 (1–2) (2011) 1–27, https://doi.org/10.1016/j.memsci.2011.03.014.
[13] P. Martins, A.C. Lopes, S. Lanceros-Mendez, Electroactive phases of poly (vinylidene fluoride): determination, processing and applications, Prog. Polym. Sci. 39 (4) (2014) 683–706, https://doi.org/10.1016/j.progpolymsci.2013.07.006.
[14] S. Munari, A. Bottino, G. Capannelli, Casting and performance of polyvinylidene fluoride based membranes, J. Membr. Sci. 16 (1983) 181–193, https://doi.org/10.1016/S0376-7388(00)81309-5.
[15] M. Gazzano, C. Gualandi, A. Zucchelli, T. Sui, A.M. Korsunsky, C. Reinhard, M. L. Focarete, Structure-morphology correlation in electrospun fibers of semicrystalline polymers by simultaneous synchrotron SAXS-WAXD, Polymer 63 (2015) 154–163, https://doi.org/10.1016/j.polymer.2015.03.002.
[16] P. Ryšánek, O. Benada, J. Tokarský, M. Syrový, P. Čapková, J. Pavlík, Specific structure, morphology, and properties of polyacrylonitrile (PAN) membranes prepared by needleless electrospinning; Forming hollow fibers, Mater. Sci. Eng. C 105 (2019) 110151, https://doi.org/10.1016/j.msec.2019.110151.
[17] A. Younis, D. Chu, S. Li, Cerium oxide nanostructures and their applications, in: M. A. Farrukh (Ed.), Functionalized Nanomaterials, IntechOpen, Rijeka, Croatia, 2016, pp. 53–68.
[18] C. Sun, H. Li, L. Chen, Nanostructured ceria-based materials: synthesis, properties, and applications, Energy Environ. Sci. 5 (2012) 8475–8505, https://doi.org/10.1039/C2EE22310D.
[19] K. Reed, A. Cormack, A. Kulkarni, M. Mayton, D. Sayle, F. Klaessig, B. Stadler, Exploring the properties and applications of nanoceria: is there still plenty of room at the bottom? Environ. Sci. Nano. 1 (2014) 390–405, https://doi.org/10.1039/C4EN00079J.
[20] Y. Ma, W. Gao, Z. Zhang, S. Zhang, Z. Tian, Y. Liu, J.C. Ho, Y. Qu, Regulating the surface of nanoceria and its applications in heterogeneous catalysis, Surf. Sci. Rep. 73 (1) (2018) 1–36, https://doi.org/10.1016/j.surfrep.2018.02.001.
[21] C.T. Campbell, C.H.F. Peden, Oxygen vacancies and catalysis on ceria surfaces, Science 309 (2005) 713–714, https://doi.org/10.1126/science.1113955.
[22] Tana, M. Zhang, J. Li, H. Li, Y. Li, W. Shen, Morphology-dependent redox and catalytic properties of CeO_2 nanostructures: nanowires, nanorods and nanoparticles, Catal. Today 148 (1–2) (2009) 179–183, https://doi.org/10.1016/j.cattod.2009.02.016.
[23] J. Stubenrauch, E. Brosha, J.M. Vohs, Reaction of carboxylic acids on CeO_2(111) and CeO_2(100), Catal. Today 28 (4) (1996) 431–441, https://doi.org/10.1016/S0920-5861(96)00251-9.
[24] Z. Wang, Z. Chen, J. Zheng, S. Zuo, Effect of particle size and crystal surface of CeO_2 on the catalytic combustion of benzene, Materials 13 (2020) 5768, https://doi.org/10.3390/ma13245768.
[25] Y. Yoshida, Y. Arai, S. Kado, K. Kunimori, K. Tomishige, Direct synthesis of organic carbonates from the reaction of CO_2 with methanol and ethanol over CeO_2 catalysts, Catal. Today 115 (1–4) (2006) 95–101, https://doi.org/10.1016/j.cattod.2006.02.027.
[26] C. Zhu, X. Wei, W. Li, Y. Pu, J. Sun, K. Tang, H. Wan, C. Ge, W. Zou, L. Dong, Crystal-plane effects of $CeO_2\{110\}$ and $CeO_2\{100\}$ on photocatalytic CO_2 reduction: synergistic interactions of oxygen defects and hydroxyl groups, ACS Sustain. Chem. Eng. 8 (38) (2020) 14397–14406, https://doi.org/10.1021/acssuschemeng.0c04205.
[27] Y. Huang, C.F. Yan, C.Q. Guo, Y. Shi, Experimental and first-principles DFT study on oxygen vacancies on cerium dioxide and its effect on enhanced photocatalytic hydrogen production, Int. J. Hydrogen Energy 41 (19) (2016) 7919–7926, https://doi.org/10.1016/j.ijhydene.2015.10.151.
[28] B. Choudhury, A. Choudhury, Ce^{3+} and oxygen vacancy mediated tuning of structural and optical properties of CeO_2 nanoparticles, Mater. Chem. Phys. 131 (3) (2012) 666–671, https://doi.org/10.1016/j.matchemphys.2011.10.032.
[29] P. Dutta, S. Pal, M.S. Seehra, Y. Shi, E.M. Eyring, R.D. Ernst, Concentration of Ce^{3+} and oxygen vacancies in cerium oxide nanoparticles, Chem. Mater. 18 (21) (2006) 5144–5146, https://doi.org/10.1021/cm061580n.
[30] S. Deshpande, S. Patil, S.V.N.T. Kuchibhatla, S. Seal, Size dependency variation in lattice parameter and valency states in nanocrystalline cerium oxide, Appl. Phys. Lett. 87 (2005) 133113, https://doi.org/10.1063/1.2061873.
[31] J.M. López, A.L. Gilbank, T. García, B. Solsona, S. Agouram, L. Torrente-Murciano, The prevalence of surface oxygen vacancies over the mobility of bulk oxygen in nanostructured ceria for the total toluene oxidation, Appl. Catal. B Environ. 174–175 (2015) 403–412, https://doi.org/10.1016/j.apcatb.2015.03.017.
[32] K.J. Klabunde, J. Stark, O. Koper, C. Mohs, D.G. Park, S. Decker, Y. Jiang, I. Lagadic, D. Zhang, Nanocrystals as stoichiometric reagents with unique surface chemistry, J. Phys. Chem. 100 (30) (1996) 12142–12153, https://doi.org/10.1021/jp960224x.
[33] A. Khaleel, W. Li, K.J. Klabunde, Nanocrystals as stoichiometric reagents with unique surface chemistry. New adsorbents for air purification, Nanostruct. Mater. 12 (1–4) (1999) 463–466, https://doi.org/10.1016/S0965-9773(99)00159-2.
[34] P. Janoš, J. Henych, O. Pelant, V. Pilařová, L. Vrtoch, M. Kormunda, K. Mazanec, V. Štengl, Cerium oxide for the destruction of chemical warfare agents: a comparison of synthetic routes, J. Hazard Mater. 304 (2016) 259–268, https://doi.org/10.1016/j.jhazmat.2015.10.069.
[35] P. Janoš, J. Henych, J. Pfeifer, N. Zemanová, V. Pilařová, D. Milde, T. Opletal, J. Tolasz, M. Malý, V. Štengl, Nanocrystalline cerium oxide prepared from a carbonate precursor and its ability to breakdown biologically relevant organophospohates, Environ. Sci.: Nano 4 (2017) 1283–1293, https://doi.org/10.1039/C7EN00119C.
[36] P. Janoš, J. Ederer, M. Došek, Some environmentally relevant reactions of cerium oxide, Nova Biotechnologica et Chimica 13 (2) (2015) 148–161, https://doi.org/10.1515/nbec-2015-0005.
[37] P. Janoš, T. Hladík, M. Kormunda, J. Ederer, M. Šťastný, Thermal treatment of cerium oxide and its properties: adsorption ability versus degradation efficiency, Adv. Mater. Sci. Eng. 2014 13 (2014) 706041, https://doi.org/10.1155/2014/706041.
[38] A. Dhall, W. Self, Cerium oxide nanoparticles: a brief review of their synthesis methods and biomedical applications, Antioxidants 7 (8) (2018) 97, https://doi.org/10.3390/antiox7080097.
[39] S.M. Hirst, A.S. Karakoti, R.D. Tyler, N. Sriranganathan, S. Seal, C.M. Reilly, Anti-inflammatory properties of cerium oxide nanoparticles, Small 5 (24) (2009) 2848–2856, https://doi.org/10.1002/smll.200901048.
[40] L.L. Wong, J.F. McGinnis, Nanoceria as bona fide catalytic antioxidants in medicine: what we know and what we want to know, Adv. Exp. Med. Biol. 801 (2014) 821–828, https://doi.org/10.1007/978-1-4614-3209-8_103.
[41] A.Y. Estevez, M. Ganesana, J.F. Trentini, J.E. Olson, G. Li, Y.O. Boateng, J.M. Lipps, S.E.R. Yablonski, W.T. Donnelly, J.C. Leiter, J.S. Erlichman, Antioxidant enzyme-mimetic activity and neuroprotective effects of cerium oxide nanoparticles

stabilized with various ratios of citric acid and EDTA, Biomolecules 9 (10) (2019) 562, https://doi.org/10.3390/biom9100562.
[42] B.C. Nelson, M.E. Johnson, M.L. Walker, K.R. Riley, C.M. Sims, Antioxidant cerium oxide nanoparticles in biology and medicine, Antioxidants 5 (2) (2016) 15, https://doi.org/10.3390/antiox5020015.
[43] Solef® 6020/1001, Solvay [online]. 2022 [cit. 2022-03-21]. Accessible from: https://www.solvay.com/en/product/solef-60201001.
[44] J. Tolasz, J. Henych, M. Šťastný, Z. Němečková, M.Š. Slušná, T. Opletal, P. Janoš, Room-temperature synthesis of nanoceria for degradation of organophosphate pesticides and its regeneration and reuse, RSC Adv. 10 (2020) 14441–14450, https://doi.org/10.1039/d0ra00937g.
[45] D. Phifer, L. Tuma, T. Vystavel, P. Wandrol, R.J. Young, Improving SEM imaging performance using beam deceleration, Microscopy Today 17 (2009) 40–49, https://doi.org/10.1017/S1551929509000170, 04.
[46] R. Hasegawa, Y. Takahashi, Y. Chatani, H. Tadokoro, Crystal structures of three crystalline forms of poly(vinylidene fluoride), Polym. J. 3 (1972) 600–610, https://doi.org/10.1295/polymj.3.600.
[47] R.W.D. Wyckoff, Crystal Structures, second ed., vol. 1, John Wiley, New York, 1965.
[48] H. Sun, COMPASS: an ab initio force-field optimized for condensed-phase applications – overview with details on alkane and benzene compounds, J. Phys. Chem. B 102 (38) (1998) 7338–7364, https://doi.org/10.1021/jp980939v.
[49] Q. Mei, C.X. Li, J.X. Wang, J.F. Chen, Y. Le, Molecular dynamics simulation on the interaction of CeO_2 and silane coupling agent in solutions, Mater. Res. Bull. 49 (2014) 265–271, https://doi.org/10.1016/j.materresbull.2013.09.001.
[50] G. Bahlakeh, B. Ramezanzadeh, M. Ramezanzadeh, Cerium oxide nanoparticles influences on the binding and corrosion protection characteristics of a melamine-cured polyester resin on mild steel: an experimental, density functional theory and molecular dynamics simulation study, Corrosion Sci. 118 (2017) 69–83, https://doi.org/10.1016/j.corsci.2017.01.021.
[51] F. Zeng, C. Peng, Y. Liu, J. Qu, Reactive molecular dynamics simulations on the disintegration of PVDF, FP-POSS, and their composite during atomic oxygen impact, J. Phys. Chem. 119 (30) (2015) 8359–8368, https://doi.org/10.1021/acs.jpca.5b03783.
[52] K.C. Satyanarayana, K. Bolton, Molecular dynamics simulations of α- to β-poly (vinylidene fluoride) phase change by stretching and poling, Polymer 53 (14) (2012) 2927–2934, https://doi.org/10.1016/j.polymer.2012.04.008.
[53] L. Pauling, The Nature of the Chemical Bond and the Structure of Molecules and Crystals: an Introduction to Modern Structural Chemistry, third ed., Cornell University Press, Ithaca, 1960.